

Regular Paper

## Unsteady Flow Visualization at Part-Load Conditions of a Radial Diffuser Pump: by PIV and CFD

Feng, J.\*, Benra, F.-K.\* and Dohmen, H.J.\*

\* Department of Mechanical Engineering, Faculty of Engineering, University of Duisburg-Essen, Duisburg, 47048, Germany. E-mail: jianjun.feng@uni-due.de

Received 13 April 2008  
Revised 17 August 2008

**Abstract:** The present study provides flow visualization on complex internal flows in a radial diffuser pump under part-load conditions by using the three-dimensional Navier-Stokes code CFX-10 with Detached Eddy Simulation (DES) turbulence model. Particle Image Velocimetry (PIV) measurements have been conducted to validate numerical results. The CFD results show good agreements with experimental ones on both the phase-averaged velocity fields and turbulence field. The detailed flow analysis shows that no separation occurs at  $0.75Q_{des}$  although a low-velocity zone develops on the rear impeller suction side. Steady flow separations are observed on the impeller suction sides at  $0.5Q_{des}$  but with different onsets and amounts. When reducing the flow rate to  $0.25Q_{des}$ , CFD predicts different types of back flows in the impeller region, including steady leading edge separations, rotating vortex in the impeller wake region, and back flow on the impeller pressure side.

**Keywords:** Flow visualization, Radial pump, PIV, CFD, Flow separation.

### 1. Introduction

Radial diffuser pumps play important roles in a wide range of industrial applications, which require that the pump system can be operated over a wide flow range. When reducing the flow rate from the design value while maintaining the pump rotating speed, the meridian velocity at the impeller inlet consequently decreases, resulting in a positive incidence angle at the impeller leading edge. Flow separation on the impeller suction sides could probably occur when the incidence angle reaches a certain threshold. In some cases, rotating stalls in the impeller passages could appear and produce non-uniform flow distribution in the circumference direction (Japikse et al., 1997).

Some studies have been conducted to investigate unsteady velocity fields in radial diffuser pumps for the design operating point, such as the numerical work by Bert et al. (1996), He and Sato (2001), Ardizzon and Pavesi (2004), Benra and Dohmen (2005). Particle Image Velocimetry (PIV) measurement is a non-contact way of measuring flow velocities and becomes very popular (Ueda, et al., 2007; Kim, et al., 2008). PIV measurements in radial pumps were also reported by Akin and Rockwell (1994), Sinha et al. (2000) and Wuibaut et al. (2002, 2004).

Rotating stall in the diffuser region of a radial pump has been observed at low flow rate by some authors, such as Sinha et al. (2001) and Sano et al. (2001) by PIV measurements, and Guleren and Pinarbasi (2004) by numerical simulation with a commercial CFD code FLUENT. Pedersen et al. (2003) found a steady stall at quarter flow rate in a vaneless impeller by PIV. Krause et al. (2005) revealed by Time-resolved PIV that the steady stall in the impeller became a rotating stall when reducing the flow rate from 50 to 41 percent of the design value.

The understanding of unsteady flow behavior in a radial pump at part-load conditions is of great importance. The main objective of the present study is investigating the unsteady flow at part-load conditions in a low specific speed radial diffuser pump. Both results from PIV measurements and CFD calculations are

presented and compared at several part-load conditions, and more attention is paid to the stall phenomenon in the impeller region.

## 2. Nomenclature

$C$	m/s	absolute velocity	$Q$	m <sup>3</sup> /s	volume flow rate
$R, r$	mm	radius	PS	-	pressure side
SS	-	suction side	Tu	-	turbulence intensity
$u$	m/s	absolute velocity in x-direction	$U$	m/s	circumferential velocity
$v$	m/s	absolute velocity in y-direction	$W$	m/s	relative velocity
$W_u$	m/s	relative circumferential velocity	$W_r$	m/s	relative radial velocity
$\beta$	deg	relative flow angle	$\theta$	deg	circumferential coordinate
$\varphi$	deg	impeller circumferential position			

### Subscripts

1	impeller inlet	2	impeller outlet
3	diffuser inlet	4	diffuser outlet
des	design operating point		

### Superscripts

—	phase averaged	'	turbulent
---	----------------	---	-----------

## 3. Numerical and Experimental Setups

### 3.1 Geometry

The simulated pump stage built for PIV measurements consists of an impeller, a vaned diffuser and a vaned return channel, with a specific speed of  $n_s=22.6$ . The impeller is shrouded with six strongly backswept blades with an exit angle of 22.5 deg relative to the tangential direction. Both the diffuser and the return channel have nine vanes. All the blades are designed in two dimensions with constant thickness of 4 mm. The whole pump is manufactured out of Plexiglas to provide optical access for the laser sheet and camera to the measuring region in PIV measurements. The geometric data and the design operating point of the pump stage are summarized in Table 1.

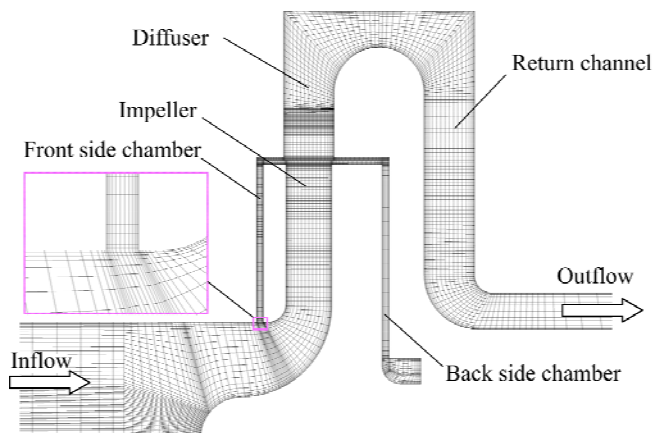


Fig. 1. Grid view in a meridional plane.

Table 1. Geometric data and operating point.

Number of impeller blades	$Z_i$	6
Impeller inlet radius	$R_1$	40 mm
Impeller outlet radius	$R_2$	75.25 mm
Number of diffuser vanes	$Z_d$	9
Diffuser inlet radius	$R_3$	77.5 mm
Diffuser outlet radius	$R_4$	95 mm
Number of return channel vanes	$Z_r$	9
Return channel inlet radius	$R_5$	95 mm
Return channel outlet radius	$R_6$	50 mm
Design volume flow rate	$Q_{des}$	0.0045 m <sup>3</sup> /s
Design rotating speed	$n_{des}$	1450 rpm
Design delivery head	$H_{des}$	7 m

### 3.2 Numerical setup

Three-dimensional unsteady flow field of the pump is solved by using the CFD code CFX-10. The structured grids for computational domains generated by ICEM-CFD 10 are shown in a meridional plane in Fig. 1. The turbulence is simulated by Detached Eddy Simulation (DES) model, which is based on the idea of covering the boundary layer by a RANS model and of switching the model to the Large Eddy Simulation (LES) mode in detached regions, in order to take some of the advantages of an LES method in detached regions with moderate computational costs (Spalart et al., 1997).

### 3.3 PIV measurement setup

The pump is driven by a motor with a maximum power of 45 kW. A 3 m<sup>3</sup> water tank feeds the water into the pump and also recollects the water out of the pump. An electromagnetic flow meter is installed on the pipe behind the pump to measure the volume flow rate. Figure 2 shows the PIV control system for image acquisition. The light source is a double-cavity 532 nm Nd-YAG laser with a repetition rate of 15 Hz. The water is seeded with polyamide particles with an average diameter of 20  $\mu\text{m}$  and a density of 1.02 relative to water. The images are recorded by a 1024  $\times$  1280 pixels camera. An encoder installed on the pump shaft is utilized to synchronize the measurements with the relative impeller positions. More details about the PIV setup can be taken from our previous work (Feng et al., 2007).

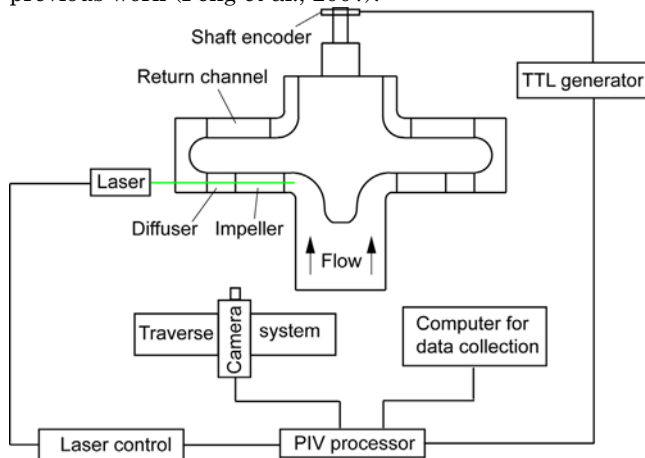


Fig. 2. PIV control system for image acquisition.

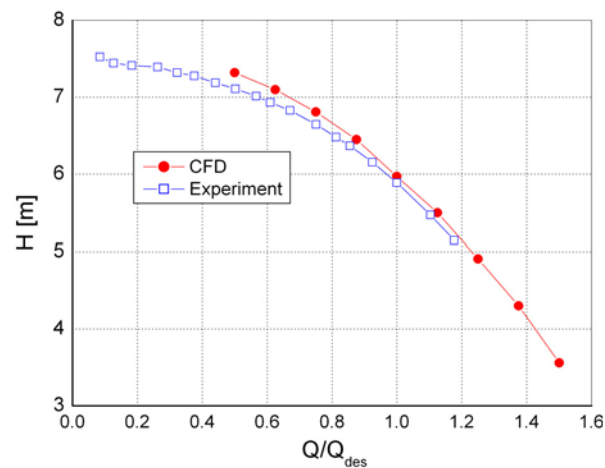


Fig. 3. Characteristic curve.

## 4. Results

In the PIV measurements, each of the measured velocity components ( $u$  and  $v$ ) in two orthogonal directions ( $x$  and  $y$ ) (see Fig. 4(b)) can be decomposed into two parts: a phase-averaged component ( $\bar{u}$  and  $\bar{v}$ ) and a fluctuating part ( $u'$  and  $v'$ ), as denoted in Eqs. (1) and (2). The phase-averaged absolute velocity  $C$  in Eq. (3) is obtained based on the phase-averaged component. The turbulence intensity  $Tu$  is calculated in Eq. (4) based on the turbulent components and normalized by the impeller tip speed  $U_2$ ,

$$u_i(x, y, \varphi) = \bar{u}_i(x, y, \varphi) + u'_i(x, y, \varphi), \quad v_i(x, y, \varphi) = \bar{v}_i(x, y, \varphi) + v'_i(x, y, \varphi) \quad i = 1, \dots, N \quad (1)$$

$$\bar{u}(x, y, \varphi) = \frac{1}{N} \sum_{i=1}^N u_i(x, y, \varphi), \quad \bar{v}(x, y, \varphi) = \frac{1}{N} \sum_{i=1}^N v_i(x, y, \varphi) \quad (2)$$

$$\bar{C}(x, y, \varphi) = \bar{u}(x, y, \varphi)\vec{i} + \bar{v}(x, y, \varphi)\vec{j} \quad (3)$$

$$Tu(x, y, \varphi) = \frac{1}{U_2} \sqrt{\frac{3}{2} \frac{1}{N} \sum_{i=1}^N \left[ \frac{1}{2} u_i'^2(x, y, \varphi) + \frac{1}{2} v_i'^2(x, y, \varphi) \right]} \quad (4)$$

where  $N=200$  is the number of instantaneous vector maps for the same impeller position, and  $\varphi$  is the impeller circumferential position. The factor 3/2 in Eq. (4) is compensating for using only two fluctuating components available in the PIV data.

All results presented here are limited to the midspan, i.e., at half blade height. The measured velocity  $\bar{C}$  in PIV is the absolute one since the camera is fixed in a stationary frame of reference. The relative velocity  $\bar{W}$  is calculated in Eq. (5) by vectorially subtracting the local circumferential velocity  $\bar{U}$  from  $\bar{C}$ . Hence:

$$\bar{W} = \bar{C} - \bar{U} \quad (5)$$

The head curves obtained by CFD and experiment are shown in Fig. 3. Obviously, the agreement is quite good. Although the result obtained by CFD is slightly higher than that by the experiment in the whole flow rate range, the biggest difference is 3%, occurring at the lowest flow rate ( $0.5Q_{des}$ ).

#### 4.1 Flow field at $0.75Q_{des}$

Figure 4(a) shows the phase-averaged relative velocity contours at one impeller position (defined as  $\varphi = 0$  deg) for the flow rate  $0.75Q_{des}$  obtained from the CFD calculation, and the PIV result is also presented in Fig. 4(b) with uniform-length vectors showing flow directions. The impeller is rotating in the clockwise direction. Obviously, two sets of data show a good agreement, although CFD predicts slightly higher velocity on the diffuser suction side in the semi-vented region. Positive incidence angles are observed at both the impeller and diffuser leading edges, and the stagnation points consequently are shifted slightly to the pressure sides. A local region with small velocities is observed near the impeller suction side at the rear part, extending to the impeller pressure side, but no flow separation occurs. Furthermore, a low-velocity zone is also found on the diffuser pressure side after the diffuser outlet throat, which is more evident in the CFD result.

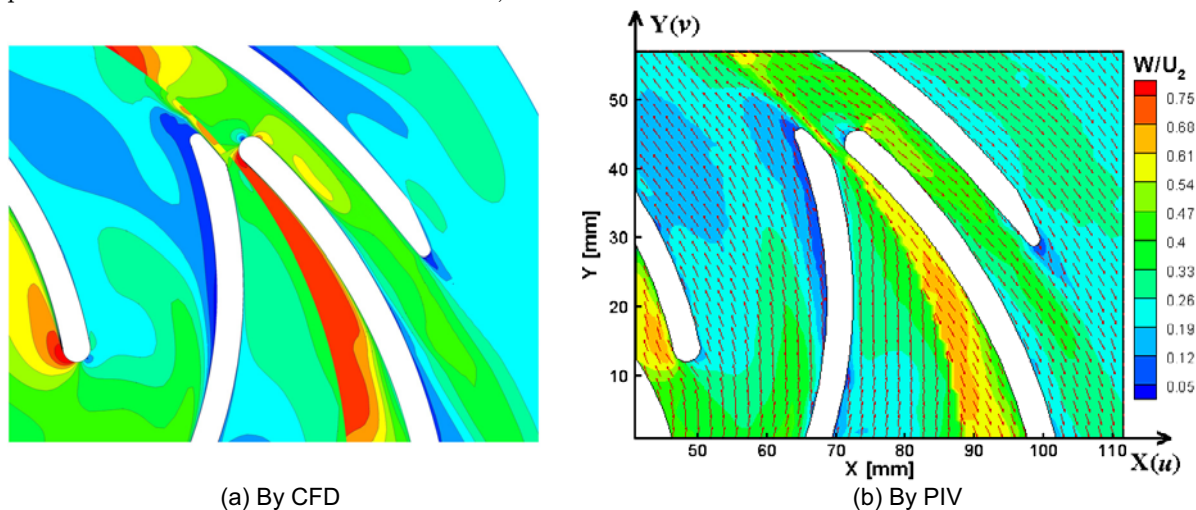


Fig. 4. Relative velocity contours at  $0.75Q_{des}$ ,  $\varphi = 0$  deg.

#### 4.2 Flow field at $0.5Q_{des}$

The phase-averaged relative velocity fields at three different impeller positions are presented at the flow rate  $0.5Q_{des}$  in Fig. 5 both by CFD calculations and by PIV measurements with the same scale. The comparison shows a very good agreement although the CFD slightly overestimates the velocities in some local small regions like the semi-vented zone in the diffuser region. In addition, the CFD results show more prominent wake near the diffuser trailing edge than the PIV results (as shown in Figs. 5(c), (d), (e) and (f)). This could be due to the moving average validation method utilized to the raw vector maps in PIV data post-process, which smoothes slightly the difference in velocity magnitudes between vectors in the wake region and surrounding vectors. For all shown positions, flow separations can be observed on the impeller suction sides. However, the onsets and amounts of the separations are quite different between two shown adjacent impeller channels. For example, the flow separation starts at about half blade chord for the blade on the right side at  $\varphi = -10$  deg (Figs. (a) and (b)), and this phenomenon keeps nearly unchanged to the next shown position  $\varphi = 10$  deg (Figs. (c) and (d)). However, the flow separation just starts near the leading edge for the left impeller blade at  $\varphi = 10$  deg, and this trend keeps developing during the following impeller positions up to  $\varphi = 26$  deg (Figs. (e) and (f)). This indicates that the non-uniformity of flow separation between channels appears in this low flow rate, but each separation zone keeps nearly unchanged during the impeller rotation by checking extensive results from CFD calculations. Therefore, the observed flow separations are steady.

Figure 6 shows the comparison of the relative velocity contours obtained from CFD in the impeller region between with and without the side chambers at  $0.5Q_{des}$  for  $\varphi = 10$  deg. It is found the flow separations are synchronous. In Fig. 6(a), stagnation points are observed at the impeller leading edges deviating to the pressure sides. However, the positions of the stagnation points are different between two adjacent impeller blades. For the two fully-shown impeller blades in Fig. 6(a), the stagnation point at the left blade is more away from the leading edge than that at the right blade, indicating different incidence angles between two blades. For the case without side chambers shown in Fig. 6(b), the stagnation points are located nearly in the identical positions, and the flow separations are very similar between two adjacent impeller channels: both start directly near the leading edge.

Figure 7 illustrates the flow field near the impeller inlet at  $r/R_1=0.95$  for the CFD result with impeller side chambers in Fig. 6(a). It can be observed that the level of radial component in impeller channel B is higher than in channel A due to the fact that the flow rate in channel B is about 70% higher than in channel A.

Consequently, the relative flow angle  $\beta = \arctan(-W_r/W_u)$  in channel A is generally smaller than in channel B (Fig. 7(b)). As a result, the incidence angles are quite different between two channels, leading to different onsets and amounts of the flow separations on the impeller suction sides mentioned above. Therefore, we can conclude that the flow in the impeller side chambers interacts with the main flow and produces non-uniform inlet condition for different impeller channels in the circumferential position.

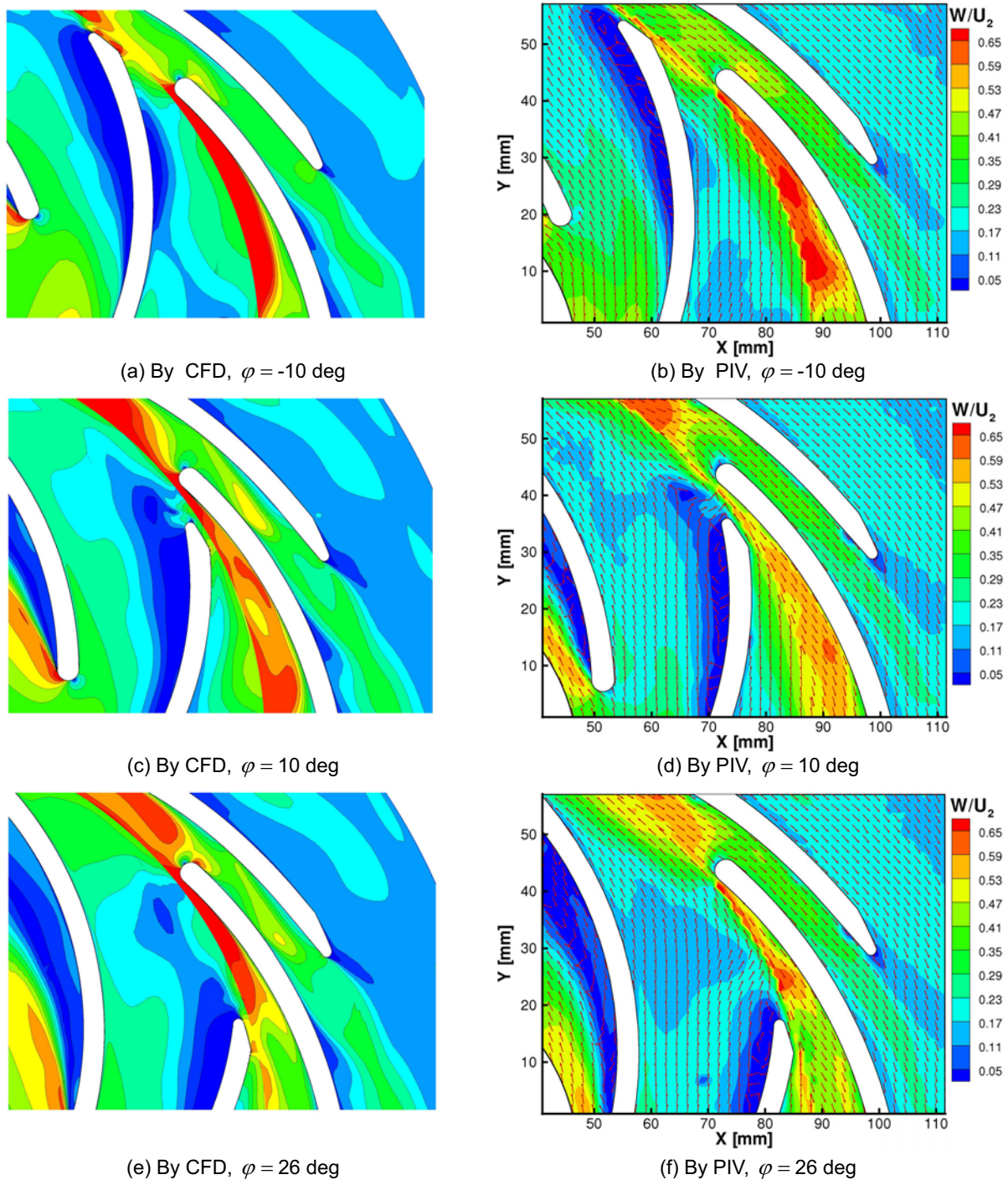


Fig. 5. Comparison of phase-averaged relative velocity fields at  $0.5Q_{des}$ .

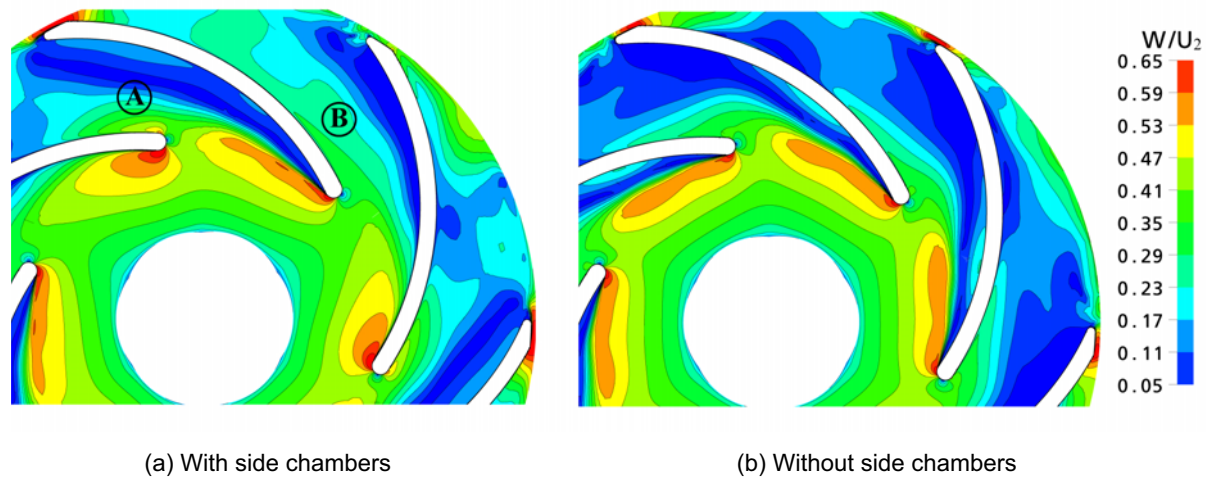


Fig. 6. Relative velocity contours at  $0.5Q_{des}$ ,  $\varphi = 10$  deg, obtained from CFD.

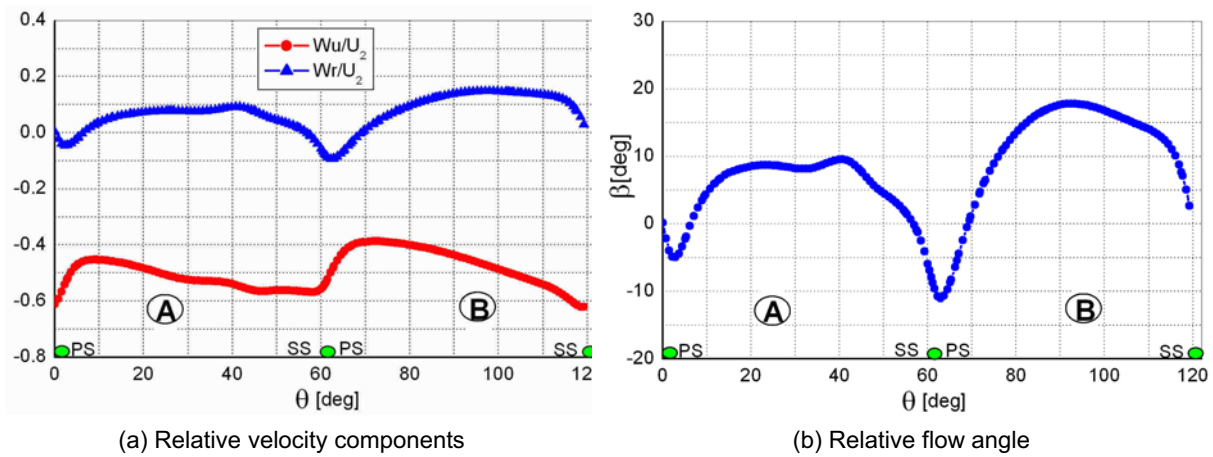


Fig. 7. Flow field near the impeller inlet at  $r/R_1=0.95$  from CFD with side chambers,  $0.5Q_{des}$ ,  $\varphi = 0$  deg.

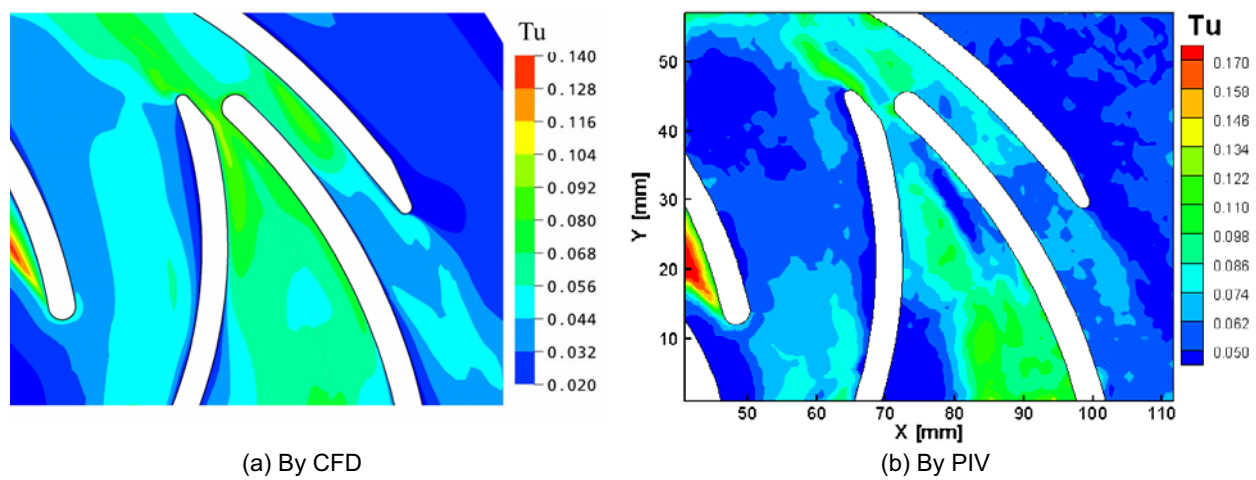


Fig. 8. Comparison of turbulence fields at  $0.5Q_{des}$ ,  $\varphi = 0$  deg.

The turbulence intensity field obtained by CFD is compared with PIV result in Fig. 8 for the impeller position  $\varphi = 0$  deg at  $0.5Q_{des}$ . Note that the scales are different: the magnitude for PIV result is 0.03 bigger than

that for CFD result for the same color, which means the turbulence for the PIV result is higher than that of CFD result. It is very clear that the turbulence level at  $0.5Q_{des}$  is generally much higher than that at the design operating point  $Q_{des}$  (Feng, 2007). Both types of results at  $0.5Q_{des}$  predict high turbulence regions on the impeller suction side near the blade leading edge caused by the leading edge separation, behind the impeller trailing edge and in the semi-vaned region of the diffuser. The highest turbulence intensity is about 13% from CFD and 17% from PIV (based on  $U_2$ ).

### 4.3 Flow field at $0.25Q_{des}$

Since CFD results have been validated by PIV measurements for the above part-load flow rates, we present here the relative velocity field for one lower flow rate  $0.25Q_{des}$ . No PIV measurements have been conducted at  $0.25Q_{des}$  due to the ceiling problem of the pump stage: water comes out of the pump from the ceilings caused by the increasing pressure field.

Figure 9 shows the relative vector plots in the impeller region for two impeller circumferential positions. Different types of back flows can be observed at this flow rate. Similar flow separations between two adjacent channels are observed on the impeller suction sides starting directly from the leading edge due to the big positive incidence angles, hardly influenced by the impeller rotation. A counter-clockwise rotating vortex is observed in the impeller wake region caused by the interaction between the impeller wake and the diffuser leading edge (Fig. 9(a)). This vortex strongly depends on the impeller position to the diffuser vane leading edge: it appears only when the diffuser leading edge is close to the impeller wake. The third type of back flow is observed near the middle of the impeller pressure side caused by the diffuser vane leading, and this back flow is strongly influenced by the relative position between the impeller and the diffuser (Fig. 9(b)).

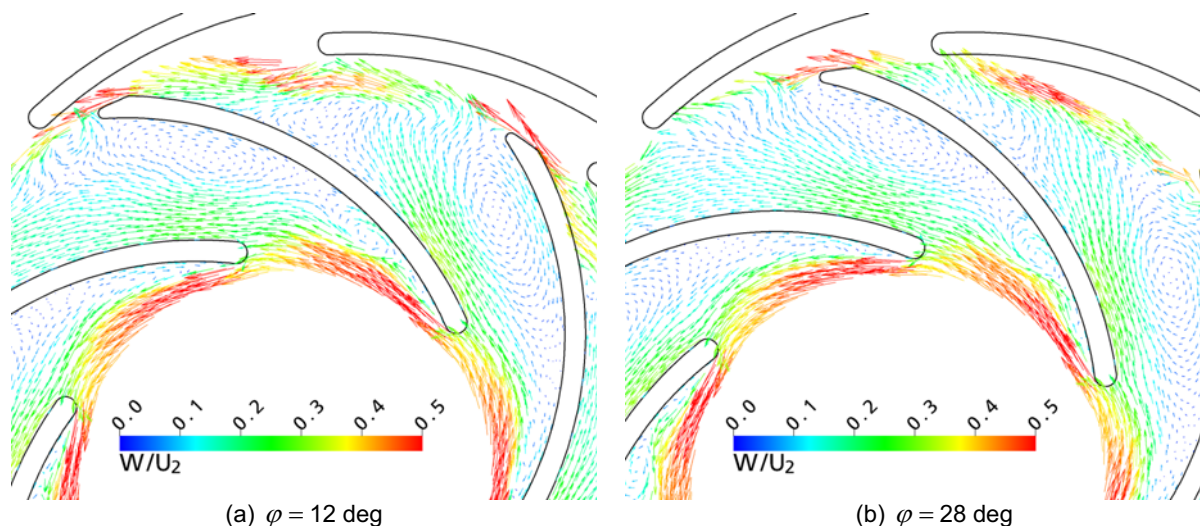


Fig. 9. Relative vector plots in the impeller region obtained by CFD,  $0.25Q_{des}$ .

## 5. Conclusions

In this paper, the unsteady flow fields at part-load conditions are studied by both CFD calculations and PIV measurements in a low specific speed radial diffuser pump, and more attention is paid to the stall phenomenon in the impeller region. The CFD results show good agreements with experiments on both the phase-averaged velocity fields and turbulence field. The detailed analysis on the flow fields shows that the flow rate has a very evident influence on the flow field. It is observed that no separation occurs at  $0.75Q_{des}$  although a low-velocity region develops on the rear impeller suction side. Steady flow separations develop on the impeller suction sides at  $0.5Q_{des}$  but with different onsets and sizes, and the highest turbulence is located on the impeller suction side near the leading edge caused by the leading edge separation there. When reducing the flow rate to  $0.25Q_{des}$ , CFD predicts different types of back flows in the impeller region, including steady leading edge separations, rotating vortex in the impeller wake region and back flow on the impeller pressure side.

## References

- Akin, O. and Rockwell, D., Flow Structure in a Radial Flow Pumping System Using High-Image-Density Particle Image Velocimetry, *ASME Journal of Fluids Engineering*, 116 (1994), 538 -554.
- Ardizzon, G. and Pavesi, G., Analysis of Unsteady Impeller Diffuser Interaction in a Centrifugal Pump, 22nd IAHR Symposium on Hydraulic Machinery and Systems, Stockholm, Sweden, June 29 - July 2, 2004.
- Benra, F.-K. and Dohmen, H. J., Numerical Investigation of the Transient Flow in a Centrifugal Pump Stage, 2005 ASME Fluids Engineering Division Summer Meeting and Exhibition, Houston, TX, USA, June 19-23, 2005.
- Bert, P. F., Combes, J. F. and Kueny, J.L., Unsteady Flow Calculation in a Centrifugal Pump Using a Finite Element Method, XVIII IAHR Symposium on Hydraulic Machinery and Cavitation, Valencia, Spain, September 16-19, 1996.
- Feng, J., Benra, F.-K. and Dohmen, H. J., Qualitative Comparison of Unsteady Flow between Numerical and Experimental Results in a Radial Diffuser Pump, *Journal of Visualization*, 10 (2007), 349-357.
- Guleren, K.M. and Pinarbasi, A., Numerical Simulation of the Stalled Flow within a Vaned Centrifugal pump, Proceedings of the IMECH E Part C Journal of Mechanical Engineering Science, 218 (2004): 425 - 435.
- Japikse, D., Marscher, W. D. and Raymond, B. F., Centrifugal Pump Design and Performance, Concepts TTI Inc., 1997.
- He, L. and Sato, K., Numerical Solution of Incompressible Unsteady Flows in Turbomachinery, *ASME Journal of Fluids Engineering*, 123 (2001), 680 - 685.
- Kim, J. S., Sung, J., Kim, S. and Kim, J. S., PIV Measurements on the Change of the Three-Dimensional Wake Structures by an Air Spoiler of a Road Vehicle, *Journal of Visualization*, 11 (2008), 45 - 54.
- Krause, N., Zaehring, K. and Pap, E., Time-Resolved Particle Imaging Velocimetry for the Investigation of Rotating Stall in a Radial Pump, *Experiments in Fluids*, 39 (2005), 192-201.
- Pedersen, N., Larsen, P. S. and Jacobsen, C. B., Flow in a Centrifugal Pump Impeller at Design and off-Design Conditions- Part I: Particle Image Velocimetry (PIV) and Laser Doppler Velocimetry (LDV) Measurements, *ASME Journal of Fluids Engineering*, 125 (2003), 61-72.
- Sano, T., Yoshida, Y. and Tsujimoto, Y., Numerical Study of Rotating Stall in a Pump Vaned Diffuser, *ASME Journal of Fluids Engineering*, 124 (2002), 363-370.
- Sinha, M. and Katz, J., Quantitative Visualization of the Flow in a Centrifugal Pump with Diffuser Vanes, Part I: on Flow Structures and Turbulence, *ASME Journal of Fluids Engineering*, 122 (2000), 97-107.
- Sinha, M., Pinarbasi, A. and Katz J., The Flow Structure During Onset and Developed States of Rotating Stall within a Vaned Diffuser of a Centrifugal Pump, *Journal of Fluids Engineering*, 123 (2001), 490 - 499.
- Spalart, P. R., Jou, W.-H., Strelets, M., and Allmaras, S. R., Comments on the Feasibility of LES for Wings and on the Hybrid RANS/LES Approach, the First AFOSR International Conference on DNS/LES, Ruston, LA, August 4-8, 1997.
- Ueda, Y., Hayashida, Y., Iguchi, M. and Ishii, T., Self-Induced Rotary Sloshing Caused by an Upward Round Jet in a Cylindrical Container, *Journal of Visualization*, 10 (2007), 317 - 324.
- Wuibaut, G., Bois, G., Dupont, P., Caignaert, G., and Stanislas, M., PIV Measurements in the Impeller and the Vaneless Diffuser of a Radial Flow Pump in Design and off-Design Operating Conditions, *ASME Journal of Fluids Engineering*, 124 (2002), 791-797.
- Wuibaut, G., Dupont, P., Caignaert, G., and Bois, G., Rotor Stator Interactions in a Vaned Diffuser Radial Flow Pump, 22nd IAHR Symposium on Hydraulic Machinery and Systems, Stockholm, Sweden, June 29- July 2, 2004.

## Author Profile



Jianjun Feng: He received his Master-degree from Xi'an University of Technology in 2002. Then he was a Ph.D student in Xi'an Jiaotong University in China. In 2008, he received his PhD-degree from University of Duisburg-Essen in Germany. His main scientific interests are rotor-stator interactions including CFD simulations and flow measurements by PIV and LDV, and optimization design of steam turbines.



Prof. F.-K. Benra: He received his PhD-degree from the Turbomachinery Institute of University Duisburg in 1986. Currently he holds the chair of Turbomachinery in University of Duisburg-Essen. His main scientific interests are rotor-stator interaction and fluid-structure interaction in all kinds of turbomachines and flow and heat transfer phenomena in secondary air systems of gas turbines.



Hans Josef Dohmen: He received his PhD-degree from the Turbomachinery Institute of University Duisburg in 1989. His main scientific interests are rotor-stator interaction and fluid-structure interaction in all kinds of turbomachines and flow and heat transfer phenomena in secondary air systems of gas turbines.